Proximal-Field Radiation Sensors

Amirreza Safaripour, Mohammed Reza M. Hashemi, and Ali Hajimiri
California Institute of Technology, Pasadena, CA 91125 USA

***Abstract*—Proximal-Field Radiation Sensors (PFRS) are introduced as a new set of tools to enable extraction of far-field radiation properties of integrated antennas from the surface waves inside their dielectric substrates. These sensors allow self-characterization, self-calibration, and self-monitoring of the radiation performance for both printed circuit board (PCB) antennas and integrated circuit (IC) antennas without any need to additional test equipment. In this paper, we explain how these sensors can be implemented and demonstrate how the far-field radiation properties can be determined from them. A PCB prototype consisting of two transmitting patch antennas and four integrated PFRS antennas is fabricated and tested to verify the concept and demonstrate the implemented sensors' capabilities to capture the radiation properties such as gain pattern, radiated polarization, and the steering angle of the antenna array as a few examples of radiation sensors applications.**

***Index Terms*—Antenna theory, dielectric substrates, electromagnetic radiation, integrated radiators, on-chip antennas, radiation detectors, sensors.**

I. Introduction

Design of antennas that are fabricated on dielectric substrates requires a thorough analysis and optimization of the electromagnetic structure. This is mainly due to the fact that dielectric substrates are excellent surface waveguides with a fundamental mode with no cutoff frequency and the integrated antennas act as the source of surface waves in the substrate [1], [2] as shown in Fig. 1(a). These surface waves that travel inside the finite substrate form the substrate modes, i.e., the electromagnetic waves that are trapped in the substrate and do not necessarily contribute to the efficient radiation. This phenomenon happens in both printed circuit board (PCB) antennas, as well as integrated circuit (IC) antennas [3]–[5] where the antenna is implemented on a dielectric substrate and thus requires a careful optimization of the substrate dimensions and permittivity to minimize the power trapped in the substrate modes. Once the integrated antennas are designed and fabricated, their testing and characterization of far-field radiation properties, as well as monitoring of their performance while in operation present a challenge. This is in part because these tasks often require use of several additional bulky pieces of equipment which exclude the possibility of in situ correction and calibration. It may also be impractical to move the antenna from its operating environment to a far-field measurement setup. Furthermore, when these antennas are integrated with the driving circuitry, either on a PCB or an IC platform, any variation of circuit components, temperature, mismatch, etc., which changes the drive circuit performance could significantly affect the antenna radiation properties, particularly in antenna arrays and multi-port antennas where the relative phases and amplitudes of the drives determine the performance [6].

In this work, we show that the surface waves that always exist in the substrate of an integrated antenna indeed contain valuable information which can be utilized to capture its far-field radiation properties, without any need to use additional test equipment and without removing the antenna from its operating environment or interfering with its operation in a wireless system. The concept of Proximal-Field Radiation Sensors (PFRS) is introduced: a number of small sensing antennas that are strategically placed and integrated on the same substrate as the transmitting antennas (Fig. 1(b)) and measure certain properties of the electromagnetic field in immediate proximity of the radiating antennas. Unlike the operational principle of traditional near-field measurement systems [7], [8], that determine the far-field patterns from measurements in the radiating near-field region of an antenna (scanning the fields outside the plane of antenna structure by an external probe), the proposed proximal-field sensors are integrated with the transmitting antennas on the same substrate and pick up information from the substrate and close proximity of transmitting antennas, and predict the far-field radiation properties of the transmitting antennas in real time, allowing for self-characterization, self-calibration, and self-monitoring of the radiation properties of the transmitting antennas.

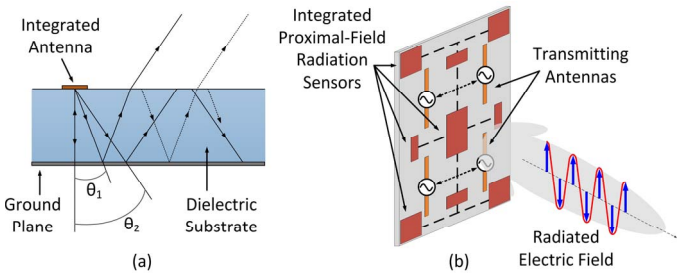

Fig. 1. (a) Generation of surface waves by integrated antenna inside the dielectric substrate and (b) proximal-field radiation sensors that pick up information contained in the excited surface waves.

II. Sensor Data Interpretation and Prototype Design

Proximal-field radiation sensors are small sensing antennas that are integrated with the transmitting antennas on the same dielectric substrate and are used to predict the far-field radiation properties in both PCB and IC antennas. These sensors are not limited to a specific shape to be functional and depending on the desired radiation properties and the transmitting

978-1-5090-6360-4/17/$31.00 ©2017 IEEE

antennas' structure, they can be of any antenna type consistent with the rest of the structure to pick up sufficient signal from the substrate. Another advantage of PFRS is that due to their proximity to the radiating source, their received signal is strong enough to enable very small sensors that can be placed anywhere on the substrate, as long as their picked-up signal level satisfies the minimum detectable signal condition for the detector circuitry attached to the sensing antennas. Depending on the desired radiation parameters, affordable circuit complexity, and choice of data processing scheme, either both amplitudes and phases or only the amplitudes of the signals from the sensing antennas may be used to determine the desired far-field radiation properties.

The data from sensors can be processed at different levels of complexity. One can simply use the structural symmetry of an electromagnetic structure and strategic placement of the sensing antennas to capture any performance deviation from the nominal design, or use simulation-based pre-defined transformations to directly convert sensors' data to the desired far-field radiation pattern. Also, various statistical methods can be used to extract existing correlation between PFRS read-outs and the desired radiation parameters.

Fig. 2 shows a proof-of-concept prototype PCB transmitter antenna array to demonstrate some basic capabilities of PFRS antennas. Two simple methods are used to interpret the data to capture various far-field radiation properties. However, it should be noted that the use of PFRS antennas and their data is not limited to the presented design and methods. The example prototype PCB antenna array consists of two transmitter patch antennas, tuned at 5 GHz, and four folded-slot PFRS antennas (followed by their output matching networks) placed symmetrically with respect to the patch antennas on the same substrate. All antennas are matched to 50Ω at 5 GHz. The structure is fully passive and there are no driver or detector circuits attached to the transmitting and sensing antennas to allow direct control of transmitter antennas drive and accurate read-out of the sensor antennas.

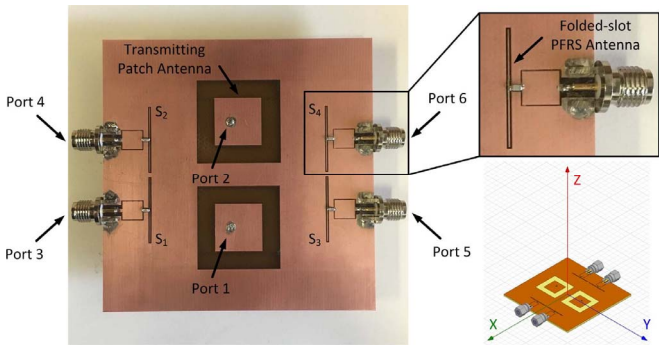

Fig. 2. The prototype PCB antenna array with two transmitting patch antennas and four folded-slot PFRS antennas.

The first parameter that we can investigate in this design is the steering angle of the far-field radiated beam in the *yz*-plane as a result of the phase difference between the patch antennas' inputs. One easy way to extract this phase difference is to monitor and compare the amplitudes of either of the sensor pairs (S_1,S_2) or (S_3,S_4) that are placed symmetrically with respect to the *x*-axis. The amplitude difference of these PFRS pairs can be used to monitor the beam steering angle of the array by tracking the drive phase difference due to symmetrical placement of the PFRS antennas.

We can also extract the mathematical relationship between the read-outs of PFRS antennas and different components of the radiated fields of the transmitting antennas (and thus the polarization of the radiated electric field) in any direction using an electromagnetic solver. Fig. 3(a) shows an example of such a simulation setup in HFSS electromagnetic solver, where a very small polarized "sniff" antenna is added to the simulation and placed at $\{\varphi = 90°, \theta = 30°\}$ direction to receive the θ-component of the radiated electric field in this direction. It can be easily shown that if the number of PFRS outputs is larger than the number of transmitting antennas' driving ports, then the phasor of the voltage picked up by the sniff antenna, V_{sniff}, which is proportional to the magnitude of the θ-component of the radiated electric field at the specified direction, can be directly calculated from the vector of PFRS read-outs' phasor voltages , $\underline{\boldsymbol{V}}_{sen}$, by a simple matrix multiplication, $V_{sniff} = T\,\underline{\boldsymbol{V}}_{sen}$, where T is a $1 \times N_s$ matrix (N_s being the number of PFRS outputs) and is formed by using the simulated S-parameters of the structure and the load impedances attached to PFRS antennas and the sniff antenna.

We can even go one step further and use the same method for all θ angles across any $\varphi = \varphi_0$ plane (shown in Fig. 3(b) for $\varphi = 90°$) to calculate both co- and cross-polarizations across this plane and combine E_φ and E_θ components to capture the entire radiation pattern across the $\varphi = \varphi_0$ plane.

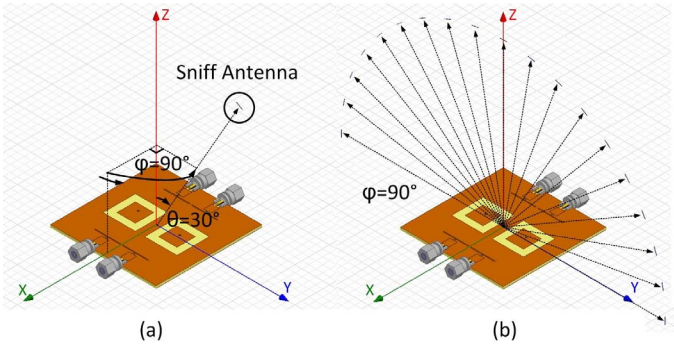

Fig. 3. Simulation setups to relate PFRS read-outs to the polarization of radiated field (a) in an arbitrary direction, and (b) across an entire plane.

It is important to note that for any type of radiating antennas, the presence of disturbing objects in the radiation path or the close vicinity of the radiator affects the far-field radiation pattern. This is mainly due to reflection and scattering from the surface of the metallic objects and the additional loss and phase shift of electromagnetic waves as they travel through disturbing dielectric materials. Furthermore, the impedance levels and electromagnetic coupling between different parts of

978-1-5090-6360-4/17/$31.00 ©2017 IEEE

the radiating structure could change significantly when the disturbing object is very close to the radiating antenna, which in turn affects the radiation performance. However, PFRS antennas are placed on the same substrate as the radiating antenna and their coupling to the excited surface waves inside the substrate is much stronger than their sensitivity to the external incident waves resulted from reflection, scattering, interference, etc. Therefore, the perturbations to the predicted radiation properties by PFRS antennas caused by disturbing objects in the radiation path and close vicinity of the radiating antennas are minimal. This makes these sensors robust in predicting the unperturbed intrinsic radiation properties of the transmitting antennas as they are not prone to disturbing objects which might have potentially introduced error to the PFRS predictions of intrinsic radiator performance.

The HFSS simulation setup depicted in Fig. 4(a) investigates an example of such a scenario for our prototype, where a $\lambda/2 \times \lambda/2$ (= 3 cm × 3 cm) metallic reflector is placed in the radiation path of the transmitting patch antennas at the vertical distance h from the PCB. Fig. 4(b) shows the top view of the same setup to clarify the relative placement of the reflector with respect to the transmitting and PFRS antennas. The normalized simulated gain patterns from HFSS across the $\varphi = 90°$ plane for the four cases of a) no reflector present, b) reflector at h = 1 cm, c) reflector at h = 6 cm, and d) reflector at h = 12 cm, are shown in Fig. 5(a). The same normalized gain patterns predicted by the simulated PFRS read-outs for the four aforementioned cases are illustrated in Fig. 5(b). A comparison between the two sets of plots reveals that although the presence of the metallic reflector affects the radiation pattern of the antenna array significantly, its effect on the PFRS prediction of the intrinsic radiation pattern is minimal.

III. Measurement

The PCB prototype shown in Fig. 2 was fabricated on a 1.6 mm thick FR4 substrate. The measured and simulated input reflection coefficients for both the transmitting and sensing antennas (S_{11} and S_{33}) are presented in Fig. 6.

Fig. 7 compares the simulated gain pattern from HFSS to the measured gain pattern by a far-field antenna pattern measurement setup and the predicted gain pattern by the measured PFRS read-outs in two orthogonal planes of $\varphi = 0°$ and $\varphi = 90°$, when the two patch antennas are driven in phase. The patterns are normalized to allow easier comparison. The predicted pattern is calculated by using the same method introduced in the previous section (using the T matrix and phasor voltages from the sensors). As it can be seen, the three radiation patterns match well, particularly in $\varphi = 90°$ plane where the radiated beam is narrower. This is further illustrated in Fig. 8 where the relative phases of the two patch antennas are switched to 90°, -90°, and 180°, respectively, to significantly change the radiation pattern in $\varphi = 90°$ plane and yet for all three cases, the simulated, measured, and sensor-predicted normalized gain patterns match very closely.

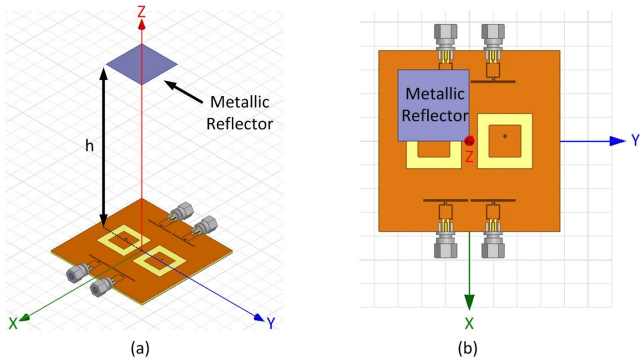

Fig. 4. Simulation setup to investigate the impact of a disturbing metallic reflector on the performance of PFRS: (a) 3-D view and (b) top view.

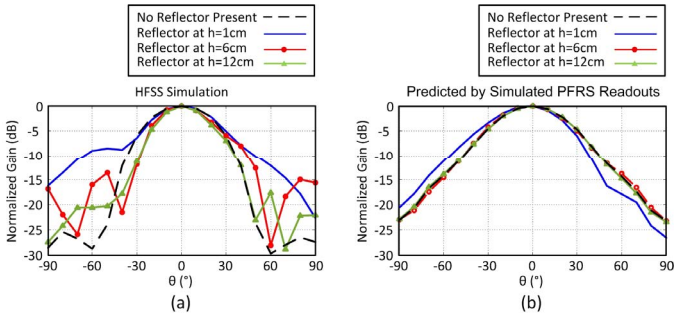

Fig. 5. Comparison of the reflector impact on the normalized gain patterns for $\varphi = 90°$ plane based on (a) HFSS simulation and (b) prediction by simulated PFRS read-outs.

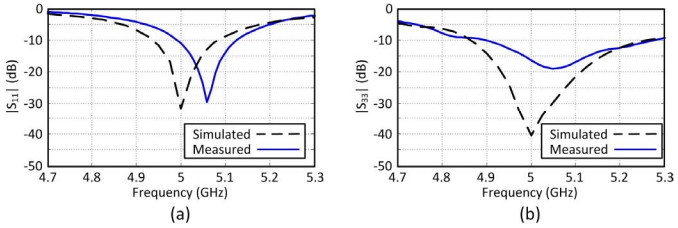

Fig. 6. Measured and simulated input reflection coefficients of (a) the patch and (b) PFRS antennas.

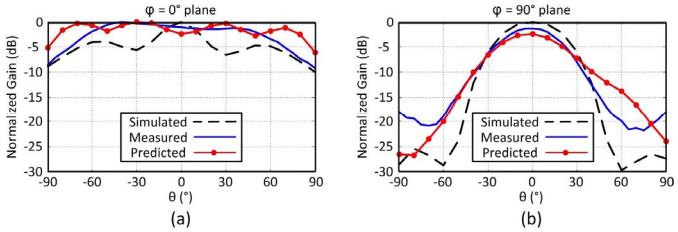

Fig. 7. Normalized simulated, measured, and predicted gain patterns based on PFRS read-outs in (a) $\varphi = 0°$ and (b) $\varphi = 90°$ planes for in-phase drive.

978-1-5090-6360-4/17/$31.00 ©2017 IEEE

As mentioned before, more specific far-field radiation properties such as polarization of the radiated electric field can also be predicted by PFRS read-outs. Fig. 9 shows the normalized simulated, measured, and predicted co- and cross-polarizations of the fabricated antenna array in φ = 90° plane to demonstrate this capability. Again, we can clearly see that PFRS prediction for the radiated polarization is well-matched to the simulation and direct polarization measurement. Finally, the simulated and measured relationship between the amplitudes of signals picked up by S_1 and S_2 PFRS antennas and the phase difference between the transmitting patch antennas as a measure to track the beam steering angle is shown in Fig. 10.

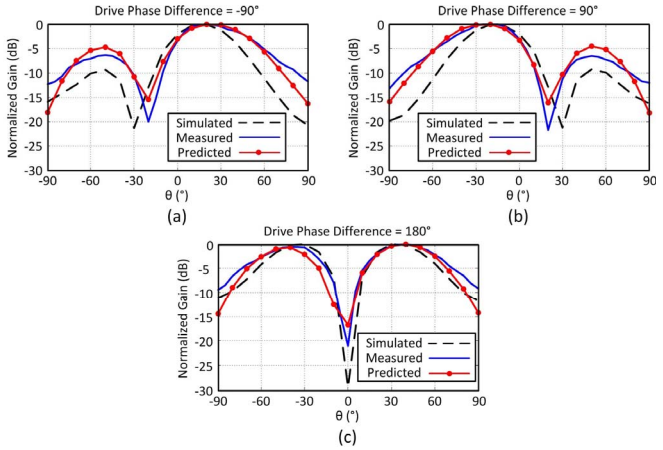

Fig. 8. Normalized simulated, measured, and predicted gain patterns based on PFRS read-outs in φ = 90° plane for (a) 90°, (b) -90° and (c) 180° of phase difference between the patch antennas.

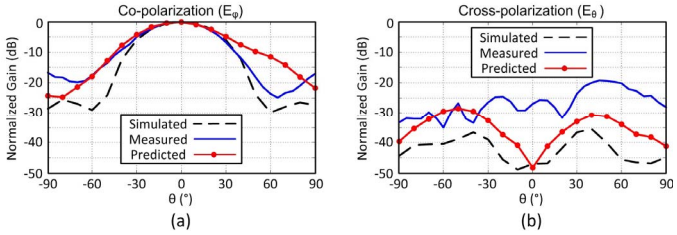

Fig. 9. Normalized simulated, measured, and predicted (a) co-polarization and (b) cross-polarization gain patterns in φ = 90° plane for in-phase drive.

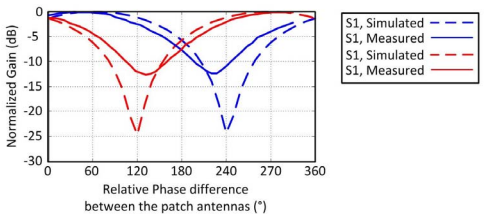

Fig. 10. Measured and simulated amplitude response of S_1 and S_2.

IV. Conclusion

The concept of integrated Proximal-Field Radiation Sensors (PFRS) is introduced as a tool to predict the far-field radiation properties of integrated antennas, based on the sensor measurements on the same dielectric substrate. These sensors use the existing information of the surface waves in the dielectric substrate to extract the desired far-field radiation properties and enable self-characterization, self-calibration and self-monitoring of the integrated antennas performance. A PCB prototype was fabricated and tested to verify the capabilities of these sensors in capturing various far-field radiation properties.

Acknowledgment

The authors would like to thank current and former members of Caltech High-speed Integrated Circuits (CHIC) laboratory and in particular Prof. Steven Bowers of University of Virginia for useful technical discussions.

References

[1] N. G. Alexopoulos, P. B. Katehi, and D. B. Rutledge, "Substrate optimization for integrated circuit antennas," *IEEE Trans. Micorw. Theory Tech.*, vol. 83, no. 7, pp. 550-557, Jul. 1983.

[2] H. Kogelnick, "Theory of dielectric waveguides," in *Integrated Optics*, T. Tamir, Ed. New York: Springer-Verlag, 1975.

[3] A. Babakhani et al., "A 77-GHz phased-array transceiver with on-chip antennas in silicon: Receiver and antennas," *IEEE J. Solid-State Circuits*, vol. 41, no. 12, pp. 2795–2806, Dec. 2006.

[4] K. Sengupta and A. Hajimiri, "A 0.28 THz power-generation and beam-steering array in CMOS based on distributed active radiators," *IEEE J. Solid-State Circuits*, vol. 47, no. 12, pp. 3013–3031, Dec. 2012.

[5] K. Sengupta and A. Hajimiri, "Designing optimal surface currents for efficient on-chip mm-wave radiators with active circuitry," *IEEE Trans. Microw. Theory Techn.*, vol. 64, no. 7, pp. 1976–1988, Jul. 2016.

[6] A. Safaripour, S. M. Bowers, K. Dasgupta, and A. Hajimiri, "Dynamic polarization control of two-dimensional integrated phased arrays," *IEEE Trans. Micorw. Theory Tech.*, vol. 64, no. 4, pp. 1066-1077, Apr. 2016.

[7] R. C. Johnson, H. A. Ecker, and J. S. Hollis, "Determination of far-field antenna patterns from near-field measurements," *Proc. IEEE*, vol. 61, pp. 1668-1694, Dec. 1973.

[8] A. D. Yaghijan, "An overview of near-field antenna measurements," *IEEE Trans. Antennas Propagat.*, vol. AP-34, pp. 30-45, Jan. 1986.

978-1-5090-6360-4/17/$31.00 ©2017 IEEE